Geochronology, 8, 313–327, 2026
https://doi.org/10.5194/gchron-8-313-2026

Response of the Rb–Sr system in biotite during contact metamorphism in the aureole of the Makhavinekh Lake Pluton, Labrador

Christopher R. M. McFarlane

Department of Earth Sciences, University of New Brunswick, Fredericton, E3B5M5, Canada

Correspondence: Christopher R. M. McFarlane (crmm@unb.ca)

Received: 18 December 2025 – Discussion started: 31 December 2025
Revised: 16 March 2026 – Accepted: 17 March 2026 – Published: 28 May 2026

Abstract. High-temperature contact metamorphism in the aureole of the 1322 Ma Makhavinekh Lake Pluton, Labrador, led to progressive consumption of 1850 Ma garnet formed during upper-amphibolite facies regional metamorphism that produced migmatitic paragneiss (Tasiyuak Gneiss). Biotite Rb–Sr isotope measurements were carried out in situ by laser ablation ICP-MS/MS allowing biotite in a variety of textural settings to be characterized. This natural laboratory provides important information about the nature of Rb–Sr closure temperature (T_c) as a function of textural setting in high-grade metamorphic rocks. Intact biotite inclusions armoured in garnet preserved in the outer aureole (> 4 km from the contact) display a range of Rb–Sr isochron ages between ∼ 1850 and ∼ 1322 Ma consistent with a zone of partial retention of Sr in biotite. Isotopic resetting in the outer aureole was controlled by microfractures in garnet that provided short-circuit diffusion pathways for redistribution of radiogenic Sr into plagioclase-bearing contact metamorphic assemblages; biotite inclusions isolated from microfractures retain 1850 Ma Rb–Sr isochron ages. Biotite grains falling along a ∼ 1322 Ma isochron attest to efficient intra- and intercrystalline Sr diffusion at $T \geq 500$ °C on timescales of ≥ 5 Myr. Samples in the central part of the contact aureole (3.7 to 1.1 km from the contact) contain partly resorbed biotite surrounded by contact metamorphic Opx + Crd coronal assemblages in addition to armoured inclusions in relict garnet. These display similar Rb–Sr behaviour to outer aureole samples with the exception that ∼ 1322 Ma biotite domains display higher Rb/Sr due to more extreme loss of Sr. In the inner aureole, where garnet was completely consumed by contact metamorphic assemblages, a new generation of biotite neoblasts grew textural equilibrium with Opx + Crd. This biotite preserves Rb–Sr ages ≤ 1322 Ma with initial $^{87}Sr/^{86}Sr$ best interpreted as a mixture of radiogenic Sr accumulated in regional biotite and whole-rock Sr liberated from low-Rb/Sr regional metamorphic garnet, apatite, and plagioclase. This study reveals how the exact textural setting of biotite in high-grade metamorphic rocks influences the preservation of Rb–Sr ages and demonstrates that there is no universal closure temperature for biotite Rb–Sr. It also reveals that in situ Rb–Sr dating of granulite-facies rocks might provide robust chronometric data if grains isolated from intergranular diffusion are systematically evaluated to reveal zones of partial retention.

1 Introduction

The closure temperature (T_c) for radiogenic Sr diffusion in biotite has been estimated primarily using empirical studies on conventional mineral separates (Hanson and Gast, 1967; Willigers et al., 2004; Armstrong et al., 1966; Percival and Peterman, 1994). Community consensus on biotite Rb–Sr closure temperatures was strongly influenced by studies such as von Blanckenburg et al. (1989), with 300 to 500 °C T_c estimates subsequently incorporated into a general knowledge framework (Chiaradia et al., 2013) and later cited in derivative publications (e.g. Nebel, 2015). Most early estimates of biotite Rb–Sr T_c attempted to contextualize variations in "open" vs. "closed" system isochron ages based on the concepts of Dodson (1973, 1979) and later modifications to volume diffusion expressions (e.g. Ehlers and Powell, 1994; Ganguly and Tirone, 1999). Recognizing the limitations of

an "infinite reservoir" model an attempt was made by Jenkin and co-workers (Jenkin et al., 2001, 1995) to review and reconcile Rb–Sr closure in biotite under "closed-system" conditions and by considering the effect of mineral modal abundance and Sr concentration on isotopic (dis)equilibrium. An important outcome of Jenkin et al. (2001, 1995) is that a fixed value for Rb–Sr closure temperature is unlikely in rocks cooling as a closed-system and with variable mineral modes (especially biotite and plagioclase) and grains sizes. However, the influence of the exact microtextural setting of biotite could not be considered using conventional analytical methods. Other studies additionally emphasized the importance of local disequilibrium affected by fluid-rock interactions (e.g. Glodny et al., 2008, and references therein). Recognizing these grain-scale controls on Rb–Sr equilibrium, attempts at micro-sampling and TIMS measurements were also made (Müller et al., 2000; Sousa et al., 2013) that revealed complexities related to the presence of older components in micas and the problem of isotopic disequilibrium in a local reactive matrix.

The advent of ICP-MS/MS technology caused a paradigm shift in how mineral chronometers relying on isobaric β-decay can be utilized. Ground-breaking papers using the laser-ablation (LA) ICP-MS/MS in situ Rb–Sr dating method (Hogmalm et al., 2017; Zack and Hogmalm, 2016) have set the stage for a reconciliation of mica closure temperatures. In cases where high-precision single-spot ages are obtained by LA MC-ICP-MS/MS (Cruz-Uribe et al., 2023; Bevan et al., 2021; Dauphas et al., 2022) or for isochron ages obtained by quadrupole-based LA ICP-MS/MS (Giuliani et al., 2024; Muñoz-Montecinos et al., 2024; Olierook et al., 2020; Glorie et al., 2024) Rb/Sr and Sr-isotope variations can now be linked to spatial and textural context, compositional variations, and microstructural features as revealed by careful optical examination or by tools such as electron-backscatter diffraction spectroscopy (EBSD) (Ribeiro et al., 2023) or laser ablation isotopic mapping (Kutzschbach and Glodny, 2024).

With the proliferation of in situ Rb–Sr mica studies there is a need to reassess closure temperatures in a variety of natural settings where physico-chemical, textural, and age information is well known. As with some of the earliest contributions to differential closure of mineral chronometers (Harrison and Clarke, 1979; Hanson and Gast, 1967), contact aureoles remain fertile testing ground for closure systematics. Here the well-characterized high-temperature aureole adjacent to the Makhavinekh Lake Pluton (MLP), Labrador, Canada, is used to test for intracrystalline Sr diffusion and the role of intergranular diffusion on biotite Rb–Sr dates. The results demonstrate that dry, diffusion-controlled, metamorphism yield characteristic behaviour in biotite Rb–Sr isotope systematics that represent one end-member of the wide range of processes likely to affect Rb–Sr closure in biotite.

2 Local geology and previous work

The MLP is part of the ca. 1350 to 1290 Ma Nain Plutonic Suite of central Labrador (Fig. 1). It is a 30 km wide (1000 km^2) composite pluton assembled at ca. 1322 Ma from successive intrusions of cumulate troctolite, anorthosite, and ferrodiorite surrounded by fayalite granite grading outward into hornblende-biotite granite (Ryan, 1991). Zircon extracted from fayalite granite samples produced a concordant TIMS U–Pb zircon age of 1322 ± 2 Ma (McFarlane et al., 2003). The MLP is in contact with the metasedimentary Tasiuyak Gneiss along its northern and southern margins. The Tasiuyak Gneiss occupies the axial region of the Torngat Orogen and is a relatively lithologically and geochemically homogeneous unit mappable over 400 km of strike length (Scott, 1998). It is a well-layered metapelitic metatexite paragneiss with alternating layers of Grt + Sil + Bt + Kfs + Qz melanosome and quartzofeldspathic leucosome (abbreviations after Whitney and Evans, 2010). The gneiss experienced peak P-T conditions of $\sim$ 850 °C and 6 to 9 kbar between 1860 to 1850 Ma (Rivers et al., 1996; Van Kranendonk, 1996; Scott and Machado, 1995; Bertrand et al., 1990; Tettelaar and Indares, 2007). These prograde assemblages were overprinted by an orogen-parallel sub-vertical mylonitic fabric with sub-horizontal lineations attributable to left-lateral shearing associated with the Abloviak Shear Zone. Subsequent exhumation and decompression of the Tasiyuak Gneiss in the northern portion of the Torngat Orogen occurred along steeply dipping east-vergent faults with exhumation constrained to the period 1790 and 1750 Ma based on Ar–Ar hornblende geochronology (Mengel and Rivers, 1997; Mengel et al., 1991). This period of near-isothermal decompression produced thin, fine-grained symplectitic coronas of Opx $\pm$ Pl on garnet and rare fine-grained Spl + Crd symplectite replacing sillimanite.

Contact metamorphism of the Tasiyuak Gneiss during intrusion of the MLP had a profound impact on the inherited regional textures and mineralogy. Several studies (McFarlane et al., 2003; Tettelaar and Indares, 2007; Kelly et al., 2011; Mariga et al., 2006) have shown that $\sim$ 1850 Ma garnet is progressively replaced by diffusion-controlled coronas comprising Opx + Pl and Opx + Crd $\pm$ Pl. The overall character of the contact metamorphic coronal assemblages and surrounding quartz-plagioclase-K-feldspar leucosome is well-illustrated using in micro-X-ray fluorescence (μXRF) mapping (Fig. 2; sample M04-450m) that reveals the localization of calcic plagioclase as part of the outermost coronal assemblage that is followed inward by symplectitic Opx + Crd. Plagioclase also locally occurs intergrown with blocky orthopyroxene that preferentially formed adjacent to quartz inclusions in garnet and quartz in the matrix bordering garnet. Thickness and grain size of coronal assemblages increases with decreasing distance to the MLP contact; the last remnants of garnet are consumed at distances < 500 m.

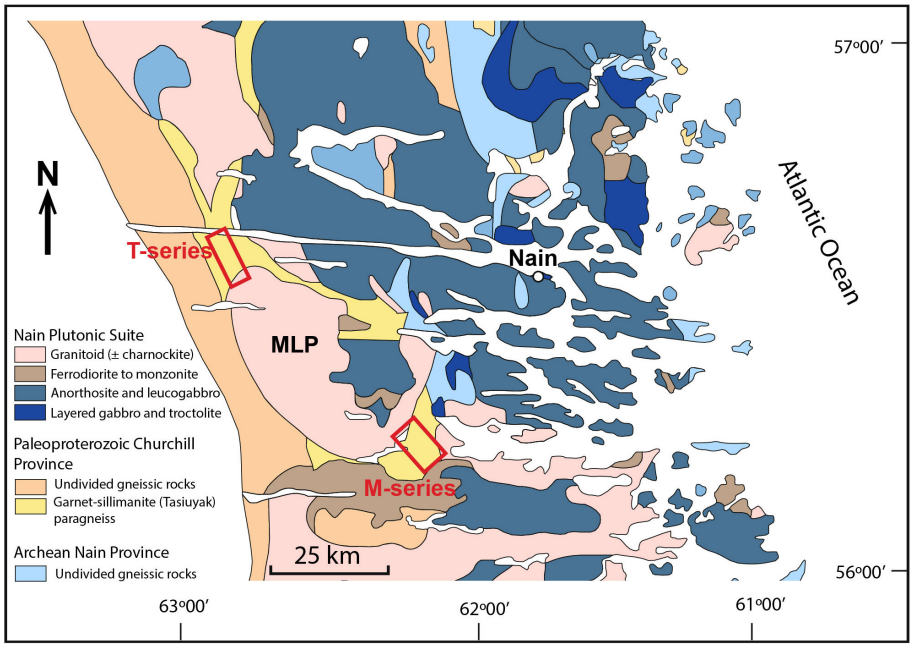

Figure 1. Location of the Makhavinekh Lake Pluton (MLP), host Tasiyuak paragneiss, and the surrounding Nain Plutonic Suite intrusions in the vicinity of Nain, coastal Labrador. Samples for this study were selected from two previously described transects from the northern (T-series samples) and southeast (M-series samples) contact zones of the MLP. Modified from Lightfoot et al. (2012).

Although the exact garnet breakdown reaction varies as a function of local bulk composition and inclusion suites, Mariga et al. (2006) envisioned a net-transfer reaction of the form: Grt + Bt + Qz = Crd + Opx + Kfs + OH. Note, however, that a new generation of biotite locally forms in textural equilibrium with Opx + Crd symplectite and this model reaction could be modified to include this biotite as an additional product acting as a sink for K, Rb, and OH. Breakdown of garnet is also accompanied by consumption of sillimanite to coarse coronal assemblages dominated by hercynitic-Spl + Crd. A less obvious transformation involved replacement of rutile by ilmenite. The composition of biotite across the MLP aureole shows only minor variability as a function of textural setting. Work by Tettelaar and Indares (2007) documented regional metamorphic biotite with XFe 0.24–0.26, 4.5 wt % to 5.7 wt % TiO_2 and predominance of F > Cl in the OH site. Contact metamorphic biotite within coronal assemblages after garnet in the inner aureole is slightly more magnesian (XFe 0.22–0.24) but with similar TiO_2 and F content owing to the similarity between peak regional temperatures and those encountered in the inner aureole. The timing of these coronal assemblages is unequivocally dated at 1322 Ma based on SHRIMP dating of neoformed Y-rich monazite that nucleated as coronal overgrowths on large pre-existing 1850 Ma grains (McFarlane et al., 2005b). Contact metamorphic temperatures in the Tasiuyak Gneiss immediately adjacent to the intrusive contact (< 100 m) reached > 800 °C as recorded by high Al concentrations in symplectitic orthopyroxene, pervasive dynamic recrystallization and polygonization of contact assemblages, and local production of anatectic melt films surrounding resorbed quartz, K-feldspar, and plagioclase. In contrast Grt-Opx, Grt-Crd, and Crd-Spl FeMg-exchange thermometry records temperatures of ∼ 575 °C at all distances in the aureole. This is interpreted as a retrograde cooling temperature and is taken as a minimum temperature achieved in the aureole.

The T-t paths, as a function of distance from the intrusive contact (assuming $P = 4$ kbar), have been previously estimated using both conductive one-dimensional analytical and multi-stage two-dimensional finite-difference models (McFarlane et al., 2003). More robust numerical modelling with convective cooling implemented in HEAT3D (Wohletz et al., 1999) indicates peak-T of 554 °C would have been reached at 6 km distance after 3.5 Myr with cooling below 500 °C after ∼ 15 Myr. Rocks in the central aureole at 3 km distance are modelled to have reached peak-T of 680 °C after 5 Myr and then cool below 500 °C after > 20 Myr. Rocks in the inner aureole would have rapidly reached peak-T > 800 °C and cooled below 500 °C after ∼ 30 Myr. Thus, biotite that remained "open" to Sr diffusion above 500 °C is expected to record isochron ages < 1310 Ma in the outer aureole and < 1295 Ma in the inner aureole.

The MLP aureole has been used to test isotopic robustness in a variety of minerals and decay systems. Zircon separated from Tasiyuak Gneiss from various distances from the contact was used to document, using SHRIMP analyses, intracrystalline redistribution of Pb during recovery of metamict domains (McFarlane et al., 2005a). Large monazite

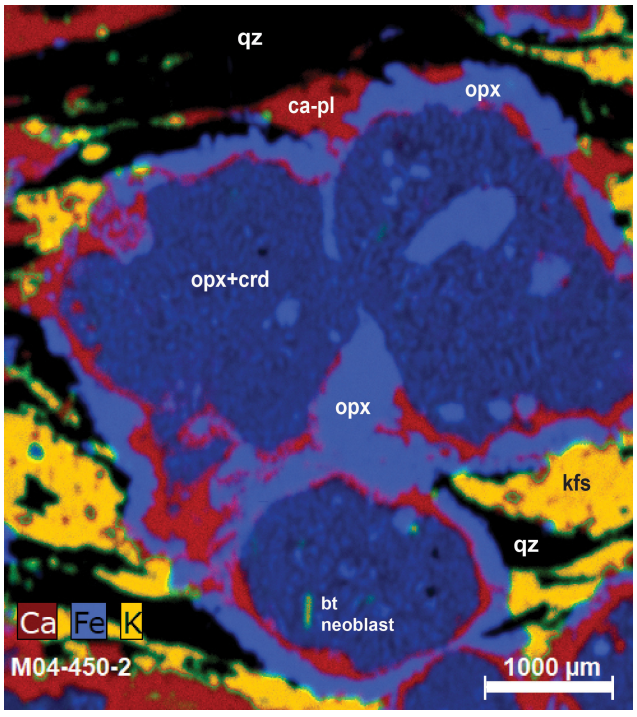

Figure 2. Micro-XRF elemental map for contact-metamorphic assemblages replacing regional metamorphic garnet in the Tasiyuak paragneiss. Sample at 450 m from contact. Tectonized leucosomes comprise deformed quartz, K-feldspar, and plagioclase. These anastomose around regional metamorphic garnet that is replaced by contact metamorphic coronal assemblages of Opx + Ca-Pl and Opx + Crd ± Bt. A biotite neoblast is present in the lowermost corona.

grains separated from the same samples were used to assess Pb-diffusion using a SIMS depth-profiling technique (McFarlane and Harrison, 2006). A combination of garnet trace-element zoning and conventional Lu–Hf geochronology was used by Kelly et al. (2011) to document the effect of garnet resorption on preservation of garnet-ilmenite Lu-Hf isochron ages. In all of these studies the progressive effects of contact metamorphism are shown to be systematic in terms of mineralogical, mineral-chemical, and isotopic changes.

3 Sample selection and description

Samples of the Tasiyuak Gneiss were examined along two transects previously documented by McFarlane et al. (2003) and Kelly et al. (2011): one approaching the northern contact of the MLP (T-series samples) the other along its southeastern margin (M-series samples) as shown in Fig. 1. Triage of the samples showed that the M-series preserves fresher assemblages containing biotite suitable for this study. Two samples < 5 m from the contact were also included from the T-series suite. The samples were chosen to include a common regional metamorphic assemblage containing Grt-Sil-Bt-Kfs-Pl-Qz with accessory rutile/ilmenite, monazite, zircon, apatite and rare pyrrhotite. The Supplement contains UTM coordinates for the samples investigated (Zone 20, Canadian NTS zone 014D).

The selected samples are divided into four groups based on distance from the intrusion (given in m from contact), textures, and contact metamorphic mineral assemblages: (1) M12-4025m, T02-4560m and T03-5750m in the outer aureole with preserved regional assemblages containing biotite armoured in garnet and pristine rutile; (2) M10-3700m, M09-2380m, and M20A-1100m at intermediate distances with partly-consumed garnet and biotite liberated to the coronal assemblages and well-preserved rutile; (3) T28-2m, M02C-10m and T08-15m from the inner aureole with biotite neoblasts in textural equilibrium with the contact metamorphic assemblages; (4) T28-2m additionally contains biotite that forms an intergranular melt-pseudomorph film between ovoid quartz and feldspars.

Plane light photomicrographs of the four main textural groups are illustrated in Fig. 3 with more detailed backscattered electron (BSE) images compiled in Fig. 4. Samples from the outer aureole (Fig. 3a) contain large garnet porphyroblasts with clustered inclusions of fine sillimanite needles that locally preserved a relict S-C fabric. Garnet hosts sub-rounded inclusions of brown biotite, locally aligned with internal fabrics, ovoid to elongate quartz inclusions, rounded ilmenite, minor apatite, and rare plagioclase. Abundant microfractures in garnet are oriented at a high angle to the proto-mylonitic layering. Garnet is wrapped by layers composed of perthitic K-feldspar, minor plagioclase, ribbon quartz, coarse-grained sillimanite and dark honey-brown rutile, and patches of foliated brown biotite. Biotite also forms irregular decussate overgrowths surrounding ilmenite and within pressure shadows surrounding garnet; this biotite is assumed to be retrograde after M2 contact metamorphism and was avoided. Garnet and sillimanite in close contact (e.g. < 500 um) display growth of fine-grained coronal assemblages of hercynitic spinel and cordierite (lower left part of Fig. 3a).

Samples centrally located in the aureole (Figs. 3b and 4a and b) record the growth of thicker layered coronae around garnet and sillimanite. A monomineralic orthopyroxene corona, 50–100 µm thick, marks the boundary between garnet rims and neighbouring quartzofeldspathic matrix. Similar monomineralic orthopyroxene coronae form internally along the interface between ovoid quartz inclusions and host garnet. Symplectitic Opx + Crd ± Pl coronae occur between the remaining garnet and the outermost Opx corona. Slender prisms of orthopyroxene and intervening cordierite form perpendicular to the reacting garnet interface. Symplectitic assemblages are also preferentially developed along pre-existing microfractures. These corona assemblages ultimately intercept biotite that was previously armoured in garnet (Figs. 3b and 4a). In these settings the portion of biotite in contact with the symplectitic minerals takes on a ragged ap-

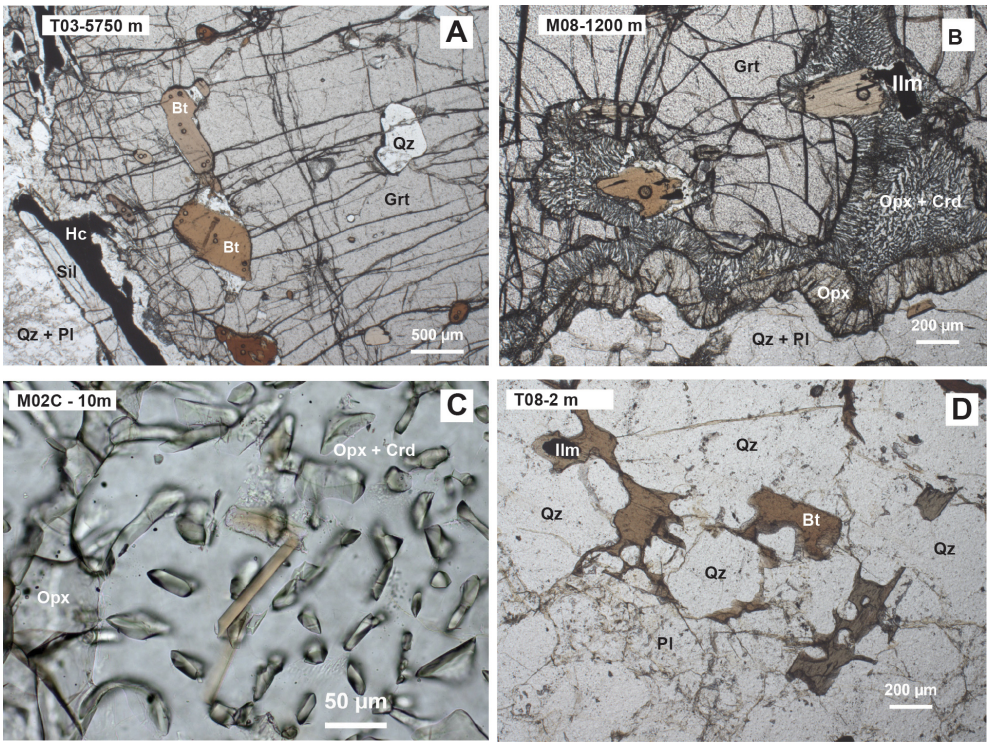

Figure 3. Plane light photomicrographs of key mineralogical and textural relationships in the MLP contact aureole. **(A)** Sample T03 from the outer aureole contains large oblate biotite and quartz inclusions in heavily microfractured garnet. Several 48 µm diameter laser craters are visible in brown biotite. **(B)** In the central part of the aureole large biotite grains can locally be found surrounded by symplectitic Opx + Crd. These grains display cuspate grain boundaries that suggest evidence of reaction. Laser craters (48 µm) also visible. **(C)** Coronal assemblages in the inner aureole locally contain subidioblastic biotite neoblasts in textural equilibrium with Opx + Crd. **(D)** Immediately adjacent to the MLP contact the Tasiyuak Gneiss displays irregular optically-continuous lobate patches of brown biotite that form interstitial domains with low dihedral angles between sub-rounded quartz and plagioclase grains.

pearance that contrasts with the smooth curvilinear boundaries of armoured biotite inclusions; the boundary is also marked by thin discontinuous grains of ilmenite (Fig. 4b). This textural difference indicates that regional biotite inclusions in garnet were destabilized when they were intersected by the M2 assemblage. Rare slender biotite also appears in central aureole samples (Fig. 4a) but are too small to analyse. The Spl + Crd symplectitic coronae around sillimanite at intermediate distances also display a layered structure, with an outer monomineralic cordierite corona surrounding a symplectitic mixture of Spl + Crd. Rutile is locally replaced by ilmenite in intermediate samples where rutile is proximal to garnet. Rutile armoured in quartz of feldspars in leucosomes remain pristine and easily identified optically.

Samples in the inner aureole (< 100 m) have no relict garnet or sillimanite preserved. Here the coronal assemblages are coarser and more randomly oriented suggesting they experienced textural reconfiguration by secondary grain growth (Figs. 3c and 4c). No relict biotite is present. Rather, platy biotite neoblasts (20–100 µm wide, up to 500 µm long) occur in textural equilibrium with Opx + Crd ± Pl ± Ilm. Biotite is rare in the layered matrix of these rocks, but it occurs in patches, locally as partially vermicular pods adjacent to coronas, that could be diagnostic of in situ melt crystallization. The quartzofeldspathic layers in the most proximal inner aureole rocks (Figs. 3d and 4d) also display evidence for partial melting such as rounded quartz and plagioclase grains surrounded by irregular grain-boundary films of biotite and K-feldspar that form with shallow dihedral angles against neighbouring grains. These are best interpreted as sites of in situ melt crystallization (so-called "melt pseudomorphs") and implies small degrees of partial melting under low aH_2O conditions at $T > 800$ °C at < 4.

4 Methods

This work was carried out using a combination of optical microscopy, laser ablation (LA) ICP-MS for trace-element quantification and in situ Rb–Sr measurement using LA ICP-MS/MS. Optical microscopy in transmitted and reflected light was used to characterize the textural setting and morphology of biotite grains as a function of proximity to the MLP intrusive contact.

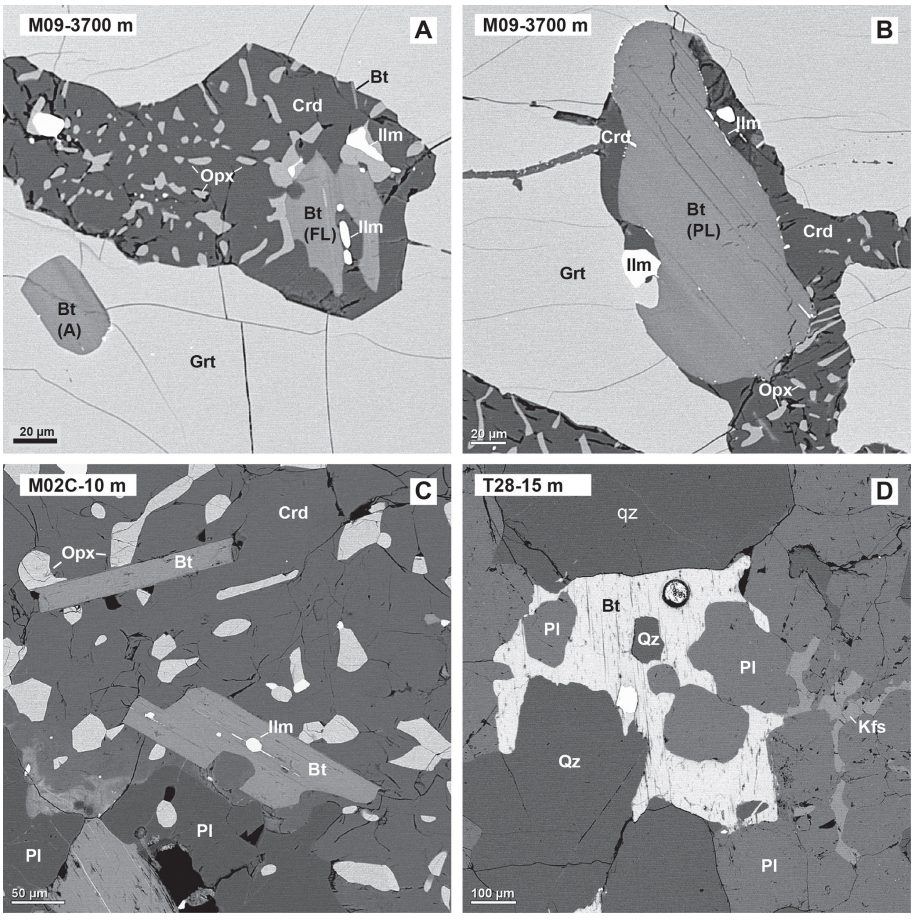

Figure 4. Backscattered electron (BSE) images of key textures and mineral assemblages in the MLP aureole. **(A)** Central aureole sample M09-3700 with armoured biotite – Bt(A) – near a previously armoured biotite that is now fully-liberated – Bt(FL) – to the M2 coronal assemblage of Opx + Crd + Ilm. **(B)** Also in sample M09-3700 large partially liberated biotite – Bt(PL) – are locally in contact with garnet and with the M2 corona and preserve a curvilinear grain boundary locally decorated by microcrystalline ilmenite. **(C)** Sample M02C-10 displays subidioblastic biotite neoblasts in textural equilibrium with coarse Opx + Crd. **(D)** In rocks at the contact with the MLP biotite and K-feldspar occur as irregular grain boundary films surrounded sub-rounded plagioclase and quartz. This texture is a hallmark of melt pseudomorphs.

The Rb–Sr isotope ratios in biotite were measured by LA ICP-MS/MS using an Applied Spectra Inc. RESOlution™ 193 nm laser system equipped with a Laurin Technic Pty. S-155 large format ablation cell that is connected to an Agilent 8900 "QQQ" ICP-MS. Laser crater diameters ranged from 66 to 26 µm depending on the size of biotite targets. Laser fluence of 1.5 to 2 J cm^{-2}, pulse rate of 7 Hz, and ablation time of 40 s were used as standard operating settings. A mixed carrier gas of pure He (300 mL min^{-1}), Ar (900 mL min^{-1}), and N_2 (1.8 mL min^{-1}) was used to transfer ablated aerosols to the mass spectrometer via two in-line Laurin Technic Pty "squid" smoothing devices. For Rb–Sr isotope measurement the Agilent 8900 was operated in in mass-shift mode using 10 % SF_6 (balance He) as the reaction gas. The analyte list included ^{39}K (10 ms), ^{44}Ca (10 ms), ^{85}Rb (10 ms), ^{104}RbF (10 ms), ^{86}Sr (20 ms), ^{105}SrF (100 ms), ^{87}Sr (10 ms), ^{106}SrF (100 ms), ^{88}Sr (10 ms), and ^{107}SrF (100 ms). The intensity of ^{87}Rb was calculated assuming a canonical ^{87}Rb/^{85}Rb of 0.38562 (Meija et al., 2016). The instrument was tuned while rastering on NIST610 to maximize counts on mass-shifted Sr while maintaining low RSD signals. This occurred at SF_6 flow rate of 28 %–30 %. Calibration of pulse/analog (P/A) factors was also carried out before each analytical session using NIST610 and an in-house apatite from Phalabowra, South Africa, with ∼ 4000 ppm Sr; this ensures that variations in ion beam intensity for mass-shifted ^{105}SrF, ^{106}SrF, and ^{107}SrF among standards and samples was fully linearized between detector modes. The signal for ^{85}Rb cps is typically counted in analog mode (> ∼ 1.4 Mcps). Net counts at mass ^{105}RbF was 0 attesting to the efficient online separation of Rb from Sr.

The S-155 cell accommodates 6 polished thin sections and 5 epoxy 25 mm diameter round standard blocks. In all analytical sessions the reference materials included

NIST610 as primary reference material (PRM), MicaMg-NP (myStandards GmbH, with reference $^{87}Sr/^{86}Sr$ value from Hogmalm et al., 2017) and an in-house phlogopite from a melanite-syenite (borolanite) from the early phase of the Loch Borralan syenite complex, Scotland (Fox and Searle, 2021; Van Breemen et al., 1979; Goodenough et al., 2011). The MicaMg-NP material was used to check accuracy of mass-bias and drift correction on mass-shifted $^{87}Sr/^{86}Sr$: the weighted mean for four analytical sessions was 1.849 ± 0.003 that overlaps the recommended value of 1.8525 ± 0.0024. Phlogopite from borolanite has a low-dispersion Rb–Sr isochron age of 415 Ma as measured independently (Adrien Vezinet, personal communication, 2025) using NIST610 and La Posta biotite (Walawender et al., 1990) as primary and matrix-correction reference material (MCRM) respectively. Each analytical session comprised 10 to 15 measurements of each certified and in-house materials that were interspersed with the unknowns. The data was reduced offline using a custom DRS in Iolite4™ (Paton et al., 2011). Dispersion for the set of drift-corrected NIST610 measurements during each run was $\sim 0.1\,\%$ for $^{87}Rb/^{86}Sr$, $\sim 0.06\,\%$ for $^{87}Sr/^{86}Sr$ and $\sim 0.05\,\%$ for $^{88}Sr/^{86}Sr$. This excess uncertainty was added to the final isotope ratios prior to matrix correction. Following the method of Glorie et al. (2024) a matrix correction factor is applied to $^{87}Rb/^{86}Sr$ to bring the Loch Borralan phlogopite in-line with the 415 Ma Rb–Sr age. This correction is then applied to the unknowns assuming similar laser-target interaction. Propagation of uncertainty from matrix correction material remains problematic for in situ Rb–Sr geochronology. In most studies, as is the case here, the range of Rb–Sr for matrix correction materials is typically < 500. For example, the range for borolanite phlogopite is ~ 3 to 80 with final isochron age uncertainty in a single run ranging from $< 2\,\%$ to $3\,\%$ depending on laser crater diameter. This contrasts with biotite in the MLP aureole with Rb/Sr that ranges from ~ 50 to > 2500 such that uncertainties on raw isochron ages (including error correlations) are routinely $< 1\,\%$ for low dispersion datasets. Propagating the full uncertainty from the matrix correction reference material isochron age is, therefore, likely to add excess uncertainty to final isochron ages for unknowns. Thus, a conservative $1\,\%$ additional uncertainty was added to final ages for MLP biotite isochrons. Initial Sr in regional metamorphic rocks was measured on plagioclase in sample T08-15m using the same methodology but with higher fluence ($5\,J\,cm^{-2}$) and NIST610 used as primary reference materials for $^{87}Sr/^{86}Sr$. The weighted mean measured value of 0.730 ± 0.002 is used to anchor isochrons when necessary. Data plotting was performed using Isoplot4.15 (Ludwig, 2012). Final isochron ages and intercepts were calculated using IsoplotR (Vermeesch, 2018) using model-1 regressions, taking into account expanded uncertainties and error correlations in the dataset. Model ages were calculated assuming initial $^{87}Sr/^{86}Sr$ of 0.73 with default uncertainty applied based on the expanded 2SE uncertainty on measured $^{87}Rb/^{86}Sr$. A sensitivity analyses showed that uncertainty on two-point model ages decrease as a function of increasing error correlation. Thus, quoted uncertainty on model ages takes into account this effect of error correlation. Data tables for Rb–Sr can be found in the Supplement.

5 Results

5.1 Armoured biotite in outer aureole

A total of 87 Rb–Sr measurements were obtained on armoured grains in outer aureole samples. The full Rb–Sr isotopic dataset is shown on a normal isochron diagram in Fig. 5. Reference isochrons for 1850 and 1322 Ma are also shown. Each of the three samples analysed at this distance contain spots on armoured grains that preserve a Rb–Sr isochron age that overlaps with the timing of $\sim$ 1850 Ma regional metamorphism. By filtering this dataset for spots with model ages > 1800 Ma it is possible to calculate a regression yielding 1824 ± 32 Ma with initial $Sr = 0.732 \pm 0.025$ (MSWD $= 1.1$; $n = 10/12$). The linearized probability plot for model ages of individual spots calculated for this dataset produces a characteristic S-shaped distribution with a slope that is far-removed from the value of 1.0 predicted for a single (normally distributed) population containing only systematic (internal) uncertainty. The oldest end of this distribution produces an anchored age of 1832 ± 26 Ma whereas the five points with youngest model ages results in an age of 1286 ± 28 Ma (MSWD $= 1.5$) and initial $Sr = 0.783 \pm 0.066$; the anchored regression age is 1297 ± 19 Ma (MSWD $= 1.7$).

5.2 Biotite liberated to coronas in central aureole

A total of 113 Rb–Sr measurements were obtained on biotite grains in three distinct textural settings in samples M10-3700m, M09-2380m, and M20A-1100m: (1) fully armoured in garnet; (2) partly liberated; (3) fully surrounded by the symplectitic coronal assemblage. The full dataset, including the linearized probability plot, is shown in Fig. 6. The distribution of Rb–Sr data in these three samples is similar to the outer aureole dataset. Only completely armoured biotite grains preserve regional metamorphic ages with the oldest subset ($n = 10$) producing an anchored isochron age of 1870 ± 25 Ma (MSWD $= 3.8$). Biotite grains that are partly liberated from garnet ($n = 31$) define an over-dispersed (MSWD $= 47$) raw regression of 1370 ± 19 Ma with initial $^{87}Sr/^{86}Sr = 0.797 \pm 0.012$. The group of four analyses with youngest model age for partly liberated grains produces an anchored isochron age of 1337 ± 20 Ma. Biotite in full contact with coronal assemblages ($n = 50$) produces a Rb–Sr age of 1330 ± 19 Ma with initial of 0.819 ± 0.012 (MSWD $= 6.7$). The five youngest model age grains in the central aureole dataset produces an over-dispersed anchored age of 1317 ± 19 Ma (MSWD $= 12$).

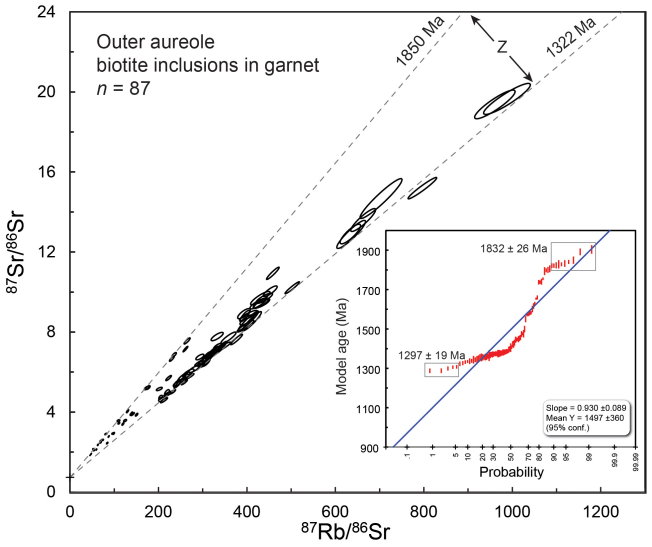

Figure 5. Rb–Sr results for biotite inclusions in garnet for outer aureole samples. Reference isochrons for 1850 and 1322 Ma were calculated at initial $^{87}Sr/^{86}Sr = 0.73$. The distribution of data points defines a zone of partial retention "Z" between these two reference lines. A gradual shift in $^{87}Rb/^{86}Sr$ to higher values accompanies resetting of 1850 Ma biotite. Inset diagram: linearized probability plot (1σ error bars) showing "S"-shaped distribution characteristic of a zone of partial retention with calculated anchored 4-point isochron for youngest analyses in this dataset.

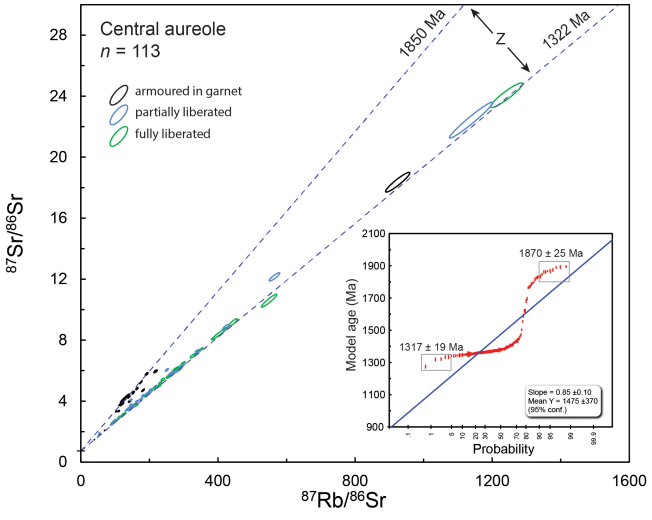

Figure 6. Rb–Sr results for central aureole. Overall, the data display a zone of partial retention similar to the outer aureole. In detail, regional metamorphic ages are recorded only by biotite grains that remained armoured in garnet. The inset linearized probability plot (1σ error bars) is similar to the outer aureole dataset and the four youngest model ages generate a low-MSWD anchored regression.

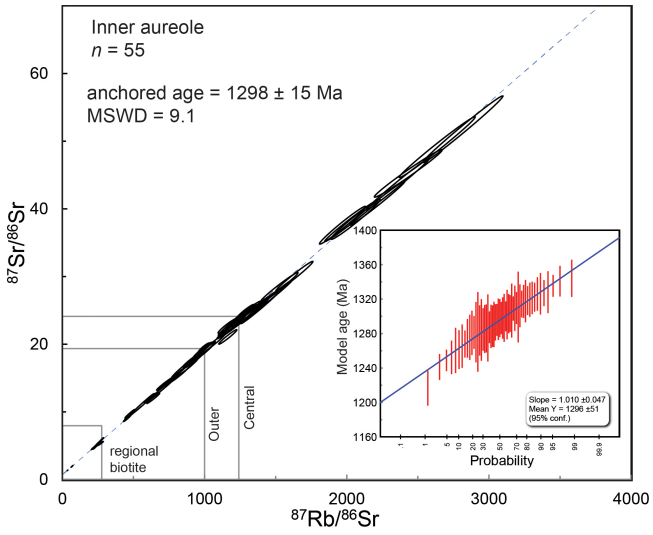

Figure 7. Rb–Sr data for neoblastic biotite grains in textural equilibrium with Opx + Crd corona in the inner aureole. Boxes show range of isotope ratios encountered in armoured regional biotite, the outer aureole and the central aureole. Inset linearized probably plot for model ages (1σ error bars) reveals a gently curving array with a slope of unity within uncertainty.

5.3 Biotite neoblasts in inner aureole

A total of 55 Rb–Sr measurements were obtained on biotite neoblasts in textural equilibrium with symplectitic assemblages in samples T08-15m, M02A-12m, and T28-2m (Fig. 7). The $^{87}Rb/^{86}Sr$ in these samples spans a range from < 50 to > 2500 and the raw regression ($n = 55$) produces an isochron of 1301 ± 19 Ma with initial $^{87}Sr/^{86}Sr = 0.703 \pm 0.011$ (MSWD = 8.8). Anchoring reduces the isochron age to 1298 ± 15 Ma (MSWD = 9.1).

Biotite neoblasts in the inner aureole also display significant inter- and intracrystalline variability in $^{87}Rb/^{86}Sr$. Exploratory $^{87}Rb/^{86}Sr$ laser mapping of large biotite inclusions in the outer aureole failed to reveal measurable heterogeneity. In contrast, biotite neoblasts large enough to accommodate multiple 26 µm diameter craters display $^{87}Rb/^{86}Sr$ that can vary by almost a factor of two from one end of the grain to the other. An example of a series of biotite neoblasts analysed in sample M02C-10m is shown in Fig. 8. The wide intracrystalline spread in $^{87}Rb/^{86}Sr$ allows calculation of single-grain ages in cases where three or more individual measurements were performed. Five grains in samples M02C-10 and one grain in T28-2m satisfied these criteria and yielded the following isochron ages when anchored at initial $^{87}Sr/^{86}Sr = 0.73 \pm 0.02$: 1285 ± 35 Ma, 1303 ± 23 Ma, 1294 ± 21 Ma, 1271 ± 22 Ma, 1285 ± 24 Ma and 1306 ± 23 Ma. The weighted mean of this population of six grains is 1294 ± 14 Ma.

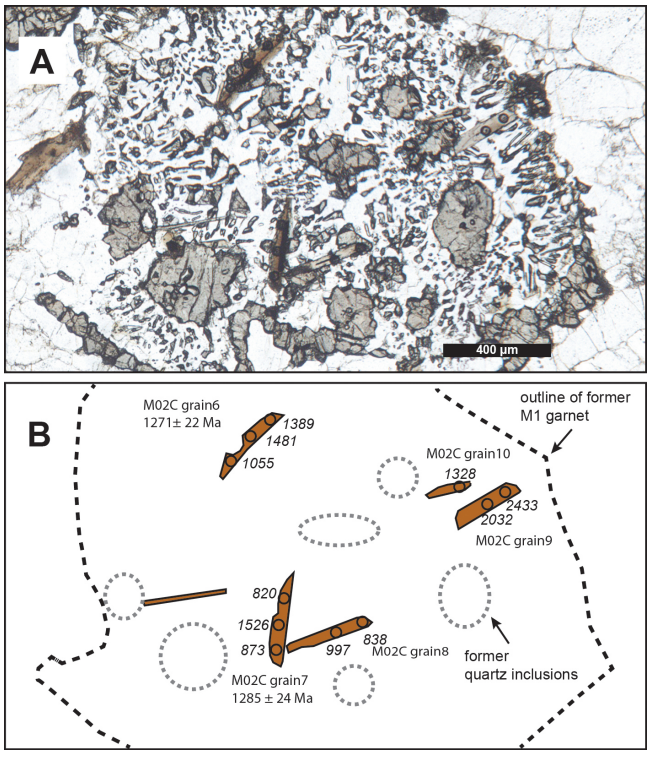

Figure 8. Detail of biotite neoblasts in inner aureole sample M02C-10. **(A)** Plane light photomicrograph showing the locations of 26 µm diameter laser craters distributed across individual grains. **(B)** Line drawing illustrating biotite neoblasts and associated $^{87}Rb/^{86}Sr$ at the laser sample locations shown by black circles. Anchored three-point isochron ages are shown for two grains.

5.4 Biotite as interstitial melt-pseudomorphs

Sample T28-2m, immediately adjacent to the intrusive contact, contains biotite and micro-perthitic K-feldspar that form as cuspate interstitial domains with low dihedral angles between sub-rounded quartz grains, a texture reminiscent of anatectic melt pseudomorph patches (e.g. Holness and Clemens, 1999). A total of 21 measurements were obtained on these domains (Fig. 9). The data fall within a narrow range of $^{87}Rb/^{86}Sr$ from ~ 400 to ~ 800 which increases uncertainty on the regression compared to the more widely dispersed Rb/Sr values in the other samples. The resulting raw isochron age is 1352 ± 38 Ma with a poorly defined initial $^{87}Sr/^{86}Sr$ of 0.53 ± 0.23 (MSWD $= 5.3$). Anchoring this dataset at 0.730 ± 0.002 produces an age of 1329 ± 17 Ma which is within uncertainty the crystallization age of the MLP. However, an initial $^{87}Sr/^{86}Sr$ of > 0.80 is required to obtain an absolute age of < 1322 Ma for these contact metamorphic melt products.

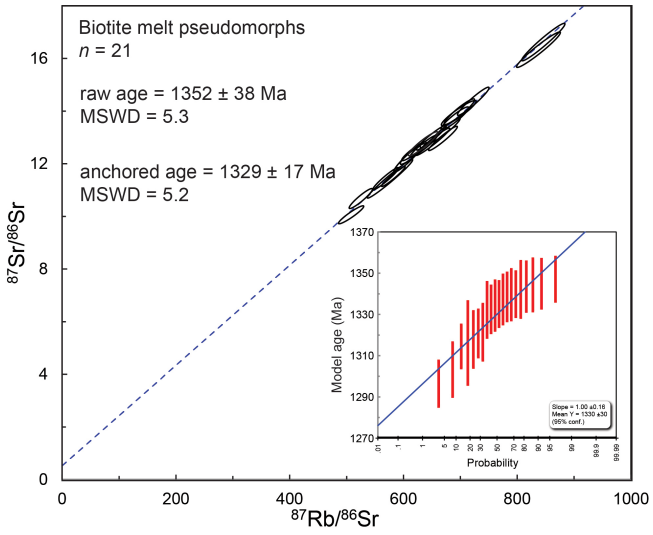

Figure 9. Rb–Sr data for biotite that occurs as melt-film pseudomorphs in Tasiyuak Gneiss at the contact with the MLP. This textural variety of biotite is characterized by a narrow range of $^{87}Rb/^{86}Sr$. The inset linearized probability curve was generated with model ages calculated at initial $^{87}Sr/^{86}Sr = 0.73$.

6 Discussion

6.1 Veracity of calculated isochron ages

The discussion of Rb–Sr behaviour in the MLP contact aureole is predicated on the accuracy of in situ Rb–Sr regressions obtained through primary standardization with NIST610 and a matrix-correction reference material (MCRM), phlogopite from a melanite-syenite "borolanite", Loch Borralan complex, Scotland, to correct for mass bias on $^{87}Rb/^{86}Sr$. The contact aureole of the MLP provides an opportunity to test the internal consistency of this standardization approach since the timing of biotite growth must have occurred at either ~ 1850 or ≤ 1322 Ma. Four analytical sessions using borolanite phlogopite produced a pooled ($n = 48$) raw regression of 381.6 ± 6.4 Ma and initial $^{87}Sr/^{86}Sr = 0.7042 \pm 0.0014$ (MSWD $= 1.2$). Some of the uncertainty in the raw age is a result of different crater sizes, and hence different laser-induced Rb/Sr fractionation, required to analyse biotite in different textural settings in the MLP aureole. Orientation effects (Larson et al., 2025) were mitigated as much as possible in both reference materials and unknowns but it is impossible to eliminate all this potential bias. The measured initial-Sr intercept overlaps within uncertainty previous whole rock measurements for Loch Borralan syenite samples by Thirlwall and Burnard (1990) that range from 0.70469 to 0.70555: all calculated isochrons for this matrix-correction phlogopite were anchored at a value of 0.7050 ± 0.0005. Reproducibility of the data reduction and correction scheme is supported by the subset of armoured biotite in the outer and central aureole ($n = 27$) that

yield an anchored isochron age of 1824 ± 32 Ma with initial $Sr = 0.732 \pm 0.025$. This age overlaps previously published conventional and in situ U–Pb 1850 Ma dates for zircon and monazite in migmatitic Tasiyuak Gneiss. The isochron initial also overlaps the $^{87}Sr/^{86}Sr$ value of 0.730 ± 0.002 independently measured on plagioclase in leucosomes. Thus, both the age and initials of corrected regressions overlap known constraints for these rocks.

6.2 Closed- vs. open-system behaviour of Sr

The zone of partial retention recorded in the outer- and central aureole samples is unequivocal evidence for intracrystalline Sr diffusion in biotite. Even some of the largest intact biotite inclusions in garnet (~ 200 µm diameter) have been reset to ~ 1322 Ma Rb–Sr ages. A petrographic examination of garnet and its armoured biotite inclusions indicates that Rb/Sr re-equilibration during contact metamorphism in the outer aureole was most likely controlled by microfractures that produced "short-circuit" diffusion pathways for Sr. Most texturally intact biotite inclusions in garnet show a systematic decrease in Sr concentration, a shift to higher Rb/Sr, and a decrease in model age towards a 1322 Ma reference line (Fig. 10). This process occurred at peak contact metamorphic temperature and timescales in the outer aureole of ~ 550 °C and a few Myr and implies efficient intra- and intercrystalline diffusion of Sr under these "dry" metamorphic conditions. There is no correlation between model age and Rb concentration observed in the outer aureole; this is consistent with the compatible nature of Rb^+ in the biotite lattice. In addition to plagioclase in the tectonized leucosomes surrounding garnet, incipient breakdown of regional 1850 Ma garnet also produced coronas that locally include calcic-plagioclase as the main host for the grossular component liberated from garnet (see Fig. 2). Acting as a host for Sr in coronas, this plagioclase provides a convenient sink for the redistribution of Sr from biotite along microfractures in the host garnet crystal; a similar source-and-sink model was advocated by Jenkin et al. (2001) in their model for Rb–Sr cation-exchange re-equilibration during cooling from lower amphibolite-facies conditions.

A simple volume-diffusion closure temperature scenario is not, however, universally applicable to biotite in the MLP aureole. For example, a sub-set of 27 analyses with model ages > 1800 Ma from armoured biotite inclusions in the outer and central aureole preserves an isochron age of 1824 ± 32 Ma that corresponds within uncertainty to zircon and monazite U–Pb ages obtained from migmatitic leucosomes in the regionally metamorphosed Tasiyuak Gniess. An important implication of this result is that it may be possible to recover prograde biotite Rb–Sr ages in upper-amphibolite to granulite facies rocks if enough grains armoured in garnet, or another refractory mineral (e.g. quartz), are analysed. Lack of isotopic resetting in these fully armoured biotite grains could reflect isolation from short-circuit pathways and slow

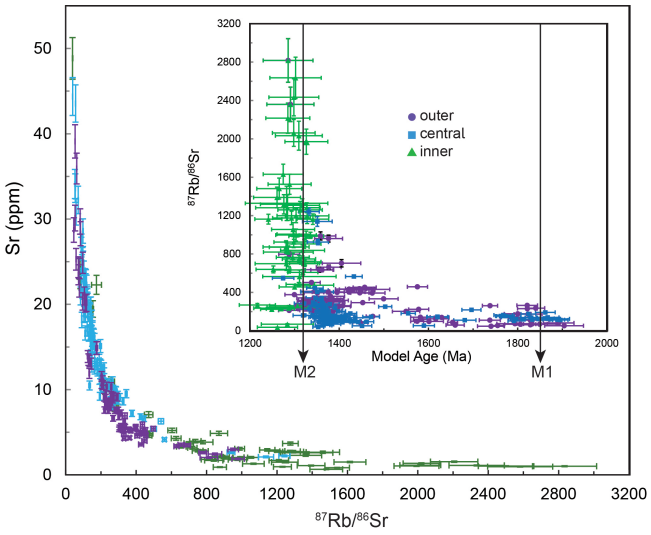

Figure 10. Concentrations of Sr in biotite decrease systematically from outer to inner aureole resulting in a progressive increase in measured $^{87}Rb/^{86}Sr$. Inset shows $^{87}Rb/^{86}Sr$ as a function of model age for each analysis (calculated assuming initial $^{87}Sr/^{86}Sr = 0.73$). Dashed vertical lines mark timing of 1850 Ma regional metamorphism and 1322 Ma MLP crystallization. Error bars are 2SE.

diffusion of Sr in garnet: Giletti (1991) estimated an 8 order of magnitude slower Sr diffusion in garnet ($\log D = -20$) compared to biotite ($\log D = -12$) at 600 °C. Thus, a universal biotite Rb–Sr closure temperature is impossible to define based on this case study since the diffusion behaviour of Sr in biotite is dependent foremost on textural setting in addition to maximum temperature, cooling rate, mineral modes, and mineral chemistry. This observation illustrates the power of in situ Rb–Sr analyses to reveal hidden details of the P-T-t history that are beyond the reach of conventional mineral separation techniques

6.3 Biotite Rb–Sr behaviour in central aureole

Biotite in the central aureole occurs in a variety of textural settings depending on the extent of corona development. Biotite analyses were categorized as having sampled: (1) armoured grains; (2) partly liberated grains; (3) fully liberated grains. Partly and fully liberated grains display cuspate grain boundaries characteristic of net-transfer reactions. Tiny (< 50 µm) biotite neoblasts are also part of the symplectitic assemblage in the central and inner aureole but are too small to analyse for in situ Rb–Sr.

Overall, the distribution of Rb–Sr data in central aureole samples is like that recorded in the outer aureole indicating similar intracrystalline and intergranular diffusion processes were at work at temperatures > 680 °C and cooling timescales of ~ 15 Myr estimated using thermal models. Armoured grains again record ~ 1850 Ma ages depending on

localized connection of biotite inclusions with through going microfractures. The combination of Rb/Sr data, single-spot model ages, textures, and concentration data provide additional evidence for Sr diffusion as the main process accounting for resetting of Rb–Sr ages in the inner aureole. Incipient growth of biotite neoblasts and rare K-feldspar acted as a sink for Rb liberated from resorbed regional metamorphic biotite. The youngest isochron calculated for fully liberated central aureole biotite is 1294 ± 19 Ma, with this younger age consistent with timescales for heating and cooling below 500 °C in the central aureole as estimated by numerical and finite difference models. Thus, the youngest Rb–Sr isochron age in these samples provides evidence for biotite Rb–Sr T_c again in the neighbourhood of 500 °C.

6.4 Biotite Rb–Sr behaviour in inner aureole

Biotite neoblasts in the inner aureole are interpreted to have grown in textural equilibrium with the Opx + Crd symplectite assemblage as exemplified in Figs. 3c and 4c. They display high Rb/Sr ratios resulting from very low Sr content and there is no evidence of a zone of partial retention as observed in the outer and central aureole. Despite the apparently homogeneous nature of the inner aureole dataset shown in Fig. 7, there is still a broad range of model ages ranging from 1344 ± 43 Ma to 1216 ± 41 Ma indicating there are other process at work beyond a simple diffusive closure mechanism. The T-t paths modelled for the inner aureole predict rapid heating to > 800 °C followed by slow cooling below 500 °C after > 25 Myr. Hence biotite neoblasts would be expected to record Rb–Sr ages < 1300 Ma if Sr diffusion was efficient above 500 °C; the pooled anchored isochron age is 1298 ± 15 Ma. The nuance in this inner aureole dataset is that individual neoblasts record strongly diffusion-controlled incorporation of Rb and Sr leading to grain-scale variations in $^{87}Rb/^{86}Sr$ such that the length scale of Rb and Sr diffusion during biotite neoblast growth was apparently shorter than the radius of a platy biotite grain (e.g. < 200 µm). Short diffusive lengthscales in the inner aureole is broadly consistent with work by Carlson (2010) who calculated seven orders of magnitude slower diffusion for Al in anhydrous versus fluid-saturated systems. This diffusion-controlled regime leads to two important processes that may not be recorded in the outer and central aureole: (1) each biotite neoblast could have crystallized with a unique initial $^{87}Sr/^{86}Sr$ depending on the precursor mineralogy of the microdomain in which it nucleated; (2) slow intergranular diffusion could effectively armour biotite neoblasts from diffusive loss of Sr.

The possibility of a unique initial Sr for each neoblast arises from the fact that ∼ 1850 Ma regional metamorphic biotite inclusions with Rb/Sr between 50 and 100 would have ingrown Sr* to produce $^{87}Sr/^{86}Sr$ between 1.7 and 2.6 by 1322 Ma. Over the same ∼ 530 Myr time interval, low Rb/Sr phases like garnet, apatite, and plagioclase would barely evolve above $^{87}Sr/^{86}Sr = 0.73$. For example, Sousa et al. (2013) reports $^{87}Rb/^{86}Sr$ in garnet that averages ∼ 0.10 with Sr concentrations between 0.1 and 100 ppm. Apatite in metamorphic settings typically contains 100–1000 ppm Sr (Tan et al., 2023; Bruand et al., 2017) and plagioclase analysed for initial $^{87}Sr/^{86}Sr$ in the MLP aureole contains 300 ± 40 ppm total Sr. Thus, biotite neoblasts that nucleated within a microdomain formerly occupied by a regional biotite inclusion might be expected to contain initial Sr significantly more radiogenic than the whole rock value. In contrast, biotite neoblasts nucleating away from these microdomains may have incorporated initial Sr closer to the whole rock. In this scenario the biotite neoblasts measured in a number of different coronas and across different samples might show a continuous range of initial $^{87}Sr/^{86}Sr$ between the whole rock value (0.73) and more radiogenic compositions. To test this scenario, it is possible to estimate the initial Sr value (I^*_{Sr}) required to lower isochron ages to ∼ 1300 Ma necessitated by slow cooling from > 800 to < 500 °C in the inner aureole. For example the subset of analyses ($n = 10$) for neoblasts with model ages > 1320 Ma yields a raw regression of 1321 ± 27 Ma and initial $^{87}Sr/^{86}Sr = 0.84 \pm 0.17$ (MSWD = 0.83). Reducing the absolute age of this regression to ∼ 1300 Ma requires an initial $^{87}Sr/^{86}Sr$ of > 1.0. This type of behaviour is not expected in the outer and central aureoles where diffusive loss of Sr from biotite would not be expected to change the initial Sr value in relict regional biotite grains.

The evidence for short diffusive length scales for Rb and Sr during neoblast growth has implications for closure of Sr diffusion in the inner aureole. Biotite neoblasts are typically surrounded by vermicular low-Ca Opx + Crd neither of which has been studied for Sr volume diffusion at $T >$ 800 °C (mostly owing to incompatible nature of large Sr^{2+} cation in these phases). However, Sr diffusion in diopside is better studied and extrapolates to $\log D < -23$ at $T < 900$ °C (Sneeringer et al., 1984): this diffusivity is slower than experimental data for Sr diffusion in garnet. It is possible, therefore, that older model ages recorded by inner aureole biotite neoblasts reflect armouring within the Opx + Crd assemblage where, because of slow diffusivity and "dry" grain boundaries, both intracrystalline and intergranular diffusion were sluggish.

The anchored isochron age of 1298 ± 15 Ma for inner aureole neoblasts could easily be taken at face value. Unfortunately, the processes described above preclude this simple interpretation. It is more likely that individual biotite neoblasts record Rb–Sr ages ranging from ∼ 1300 to 1322 Ma depending on where they occur relative to precursor mineral domains and when, relative to the thermal pulse, the grains were isolated from intergranular Sr mobility. This scenario is analogous to the continuous mixing model described by Davies et al. (2018) in which analyses with a range of initials yields a precise but ultimately meaningless average isochron age.

6.5 Inner aureole biotite melt-pseudomorphs

Finally, biotite that forms as melt-pseudomorph films in sample T28-2m reveal contrasting behaviour compared to biotite neoblasts. As shown in Figs. 3d and 4d above, these cuspate biotite films envelope sub-rounded quartz (and more rarely plagioclase) indicating that the latter was consumed during melt production. Despite analyzing biotite melt-pseudomorphs over a wide area of this thin section, the range of Rb/Sr is much narrower than biotite neoblasts: Rb/Sr = 508–825 with a mean of 637 ± 83 (1σ; 13 %) for melt films compared to 38–2800 with mean of 1270 ± 675 (1σ; 53 %) for biotite neoblasts in sample M02C-10m. The most obvious process that could account for the more homogeneous Rb–Sr in biotite melt films is the longer-range three-dimensional connectivity of melt pockets, faster diffusion of Rb and Sr through silicate melts, and the mobile nature of high-T silicate melt allowing for advective mixing. These features would promote elemental and isotopic homogenization at the scale of cm rather than µm and over timescales of a few Myr at $T > 800$ °C in the inner aureole. The narrow range of Rb/Sr places more importance on the correct choice for initial $^{87}Sr/^{86}Sr$. At this distance in the aureole, the biotite must have crystallized at ≤ 1322 Ma and this necessarily restricts the initial $^{87}Sr/^{86}Sr$ to ≥ 0.80. Efficient intercrystalline Sr diffusion at $T > 800$ °C would also promote open-system behaviour and closure ages < 1300 Ma. There is some evidence for long-lived open-system behaviour as recorded by the five youngest spots that produce an isochron age of 1294 ± 73 Ma with initial $^{87}Sr/^{86}Sr = 0.87 \pm 0.51$. More work will be needed to check the veracity of the proposed higher initial value and for open system behaviour. The initial Sr of the low-degree partial melts recorded by these biotite melt pseudomorphs could, for instance, reflect the balance and abundance of K-feldspar + biotite relative to plagioclase + quartz in the melting reaction: melting higher proportions of K-feldspar + biotite would produce more radiogenic initial $^{87}Sr/^{86}Sr$. This process is envisioned to represent the incipient stage in the eventual accumulation of anatectic melt into larger isotopically homogeneous granitic plutons. Higher-than-expected initial $^{87}Sr/^{86}Sr$ in partial melts has also been observed in Himalayan leucogranites (Yang et al., 2022) where preferential melting of muscovite has been attributed to elevated initial Sr values.

7 Conclusions

In contrast to previous studies of Rb–Sr closure in biotite, the use of in situ LA ICP-MS/MS provides unprecedented insight into the grain-scale controls on diffusion behaviour in cooling rocks. In the current study, the use of in situ Rb–Sr measurements reveals that the exact microtextural setting of biotite ultimately controlled the behaviour of the Rb–Sr system. Pervasive Rb–Sr resetting occurred only when biotite inclusions were connected to the surrounding matrix by microfractures that provided short-circuit pathways for diffusion through garnet. Open-system behaviour of Sr in biotite above 500 °C in the outer aureole is at the upper limit of Rb–Sr biotite T_c proposed by von Blanckenburg et al. (1989); it is impossible to place a lower limit on Sr diffusion in the MLP aureole but it is noteworthy that only 5 of 87 analyses in the outer aureole returned absolute model ages < 1322 Ma yet thermal models predict > 15 Myr to cool below 500 °C. This hints at T_c for Sr diffusion closer to the upper range of existing estimates.

Another key benefit of examining closure systematics in high-T contact aureoles is that confidence can be attributed to isochron ages that are significantly younger than magmatic crystallization age. Here the thermal models predict T-t paths for heating and cooling below 500 °C that span 5 to > 20 Myr depending on distance from the intrusive contact. Subsets of data that record isochron ages < 1300 Ma can be confidently attributed to open-system behaviour and canonical closure during cooling below T_c. This study also emphasizes that large datasets (e.g. > 100 spots) may sometimes be required to reveals zones of partial retention and tails on "S"-shaped linearized probability plots that could be used to calculate meaningful cooling ages. More in situ Rb–Sr dating studies in similarly well-constrained, lower-temperature, natural settings are required to expand the lower limit of Sr diffusion in biotite.

In some cases, however, 1850 Ma biotite Rb–Sr ages are preserved as long as the grains remained isolated from short-circuit diffusion. This implies that the use of biotite Rb–Sr should not be disregarded in upper-amphibolite and granulite-facies rocks: the challenge is to find biotite in textural settings (e.g. armoured grains) that may preserve prograde ages. Biotite armoured in quartz in granulite-facies rocks might be expected to display similar behaviour. Work by Tattelaar and Indares (2007) estimated regional metamorphic P-T conditions for the Tasiyuak Gneiss in the same vicinity as the present study of ~ 870 °C at 8–10 kbar and regional metamorphic biotite contains 4.5 wt % to 5.7 wt % TiO_2 and 1.91 wt % to 1.97 wt % F with only minor Cl. It is possible, therefore, that other granulite-facies and UHT rocks may contain biotite that records prograde Rb–Sr ages. Rounded biotite inclusions in peritectic minerals such as cordierite, sapphirine, orthopyroxene, and garnet (e.g. Bose et al., 2005; Guo et al., 2024) attest to dehydration of biotite sometimes at conditions > 900 °C at 8 kbar. Refined thermodynamic solution models for high-T breakdown of Ti- and Fe^{3+} biotite (e.g. Tajčmanová et al., 2009) also allow P-T pseudosection calculations in the NCKFMASHTO system; this ties armoured biotite Rb–Sr ages directly to prograde reactions in the major mineral assemblage: no such capacity currently exists for U–Pb ages from accessory minerals like zircon or monazite. Thus, demonstrating prograde Rb–Sr ages preserved in UHT biotite armoured in peritectic phases would be a valuable addition to geochronology in high-grade rocks and future work will attempt to test this hypothesis. The re-

sponse of biotite armoured in other high Rb/Sr phases like K-felspar, or low Rb/Sr phases like plagioclase could also be explored using in situ methods; these inclusion/host isotopic measurements might ultimately yield robust cooling ages if zoning profiles for Rb, Sr, Rb/Sr and $^{87}Sr/^{86}Sr$ are combined with volume diffusion data for Sr and Rb (e.g. Giletti, 1991) in these mineral pairs. Exploring such biotite (or muscovite) inclusion/host relationships using in situ methods is another fruitful avenue for further research.

Data availability. The data used in this article is available in the Supplement.

Supplement. The supplement related to this article is available online at https://doi.org/10.5194/gchron-8-313-2026-supplement.

Competing interests. The author has declared that there are no competing interests.

Disclaimer. Publisher's note: Copernicus Publications remains neutral with regard to jurisdictional claims made in the text, published maps, institutional affiliations, or any other geographical representation in this paper. The authors bear the ultimate responsibility for providing appropriate place names. Views expressed in the text are those of the authors and do not necessarily reflect the views of the publisher.

Acknowledgements. . The author acknowledges the helpful and constructive comments by two external reviewers and the guidance of the associate editor. Thanks also Adrien Vezinet for Rb-Sr analyses at ISTERRE Grenoble and to Mark Cloos for arranging shipment of the MLP sample suite from UT Austin to UNB Fredericton.

Financial support. This research has been supported by the Natural Sciences and Engineering Research Council of Canada, Networks of Centres of Excellence of Canada (grant no. RGPIN-2022-03253).

Review statement. This paper was edited by Daniela Rubatto and reviewed by Kyle Larson and one anonymous referee.

References

Armstrong, R. L., Jäger, E., and Eberhardt, P.: A comparison of K–Ar and Rb–Sr ages on Alpine biotites, Earth Planet. Sc. Lett., 1, 13–19, 1966.

Bertrand, J.-M., Van Kranendonk, M., Hanmer, S., Roddick, J. C., and Ermanovics, I.: Structural and metamorphic geochronology of the Torngat Orogen in the North River-Nutak transect area, Labrador: Preliminary results of U–Pb dating, Geoscience Canada, 1990.

Bevan, D., Coath, C. D., Lewis, J., Schwieters, J., Lloyd, N., Craig, G., Wehrs, H., and Elliott, T.: In situ Rb–Sr dating by collision cell, multicollection inductively-coupled plasma mass-spectrometry with pre-cell mass-filter,(CC-MC-ICPMS/MS), J. Anal. Atom. Spectrom., 36, 917–931, 2021.

Bose, S., Das, K., and Fukuoka, M.: Fluorine content of biotite in granulite-grade metapelitic assemblages and its implications for the Eastern Ghats granulites, Eur. J. Mineral., 17, 665–674, 2005.

Bruand, E., Fowler, M., Storey, C., and Darling, J.: Apatite trace element and isotope applications to petrogenesis and provenance, Am. Mineral., 102, 75–84, 2017.

Carlson, W.: Dependence of reaction kinetics on H_2O activity as inferred from rates of intergranular diffusion of aluminium, J. Metamorph. Geol., 28, 735–752, 2010.

Chiaradia, M., Schaltegger, U., Spikings, R., Wotzlaw, J.-F., and Ovtcharova, M.: How accurately can we date the duration of magmatic-hydrothermal events in porphyry systems? – an invited paper, Econ. Geol., 108, 565–584, 2013.

Cruz-Uribe, A. M., Craig, G., Garber, J. M., Paul, B., Arkula, C., and Bouman, C.: Single spot Rb–Sr isochron dating of biotite by LA-MC-ICP-MS/MS, Geostand. Geoanal. Res., 47, 795–809, 2023.

Dauphas, N., Hopp, T., Craig, G., Zhang, Z. J., Valdes, M. C., Heck, P. R., Charlier, B. L., Bell, E. A., Harrison, T. M., and Davis, A. M.: In situ ^{87}Rb–^{87}Sr analyses of terrestrial and extraterrestrial samples by LA-MC-ICP-MS/MS with double Wien filter and collision cell technologies, J. Anal. Atom. Spectrom., 37, 2420–2441, 2022.

Davies, J. H., Sheldrake, T. E., Reimink, J. R., Wotzlaw, J. F., Moeck, C., and Finlay, A.: Investigating complex isochron data using mixture models, Geochem. Geophy. Geosy., 19, 4035–4047, 2018.

Dodson, M. H.: Theory of Cooling Ages, in: Lectures in Isotope Geology, edited by: Jäger, E. and Hunziker, J. C., Springer, Berlin, Heidelberg, https://doi.org/10.1007/978-3-642-67161-6_14, 1979.

Dodson, M. H.: Closure temperature in cooling geochronological and petrological systems, Contrib. Mineral. Petr., 40, 259–274, 1973.

Ehlers, K. and Powell, R.: An empirical modification of Dodson's equation for closure temperature in binary systems, Geochim. Cosmochim. Ac., 58, 241–248, 1994.

Fox, R. and Searle, M. P.: Structural, petrological, and tectonic constraints on the Loch Borralan and Loch Ailsh alkaline intrusions, Moine thrust zone, northwestern Scotland, Geosphere, 17, 1126–1150, 2021.

Ganguly, J. and Tirone, M.: Diffusion closure temperature and age of a mineral with arbitrary extent of diffusion: theoretical formulation and applications, Earth Planet. Sc. Lett., 170, 131–140, 1999.

Giletti, B.: Rb and Sr diffusion in alkali feldspars, with implications for cooling histories of rocks, Geochim. Cosmochim. Ac., 55, 1331–1343, 1991.

Giuliani, A., Oesch, S., Guillong, M., and Howarth, G. H.: Mica Rb–Sr dating by laser ablation ICP-MS/MS using an isochronous calibration material and application

to West African kimberlites, Chem. Geol., 649, 121982, https://doi.org/10.1016/j.chemgeo.2024.12198, 2024.

Glodny, J., Kühn, A., and Austrheim, H.: Diffusion versus recrystallization processes in Rb–Sr geochronology: isotopic relics in eclogite facies rocks, Western Gneiss Region, Norway, Geochim. Cosmochim. Ac., 72, 506–525, 2008.

Glorie, S., Gilbert, S. E., Hand, M., and Lloyd, J. C.: Calibration methods for laser ablation Rb–Sr geochronology: comparisons and recommendation based on NIST glass and natural reference materials, Geochronology, 6, 21–36, https://doi.org/10.5194/gchron-6-21-2024, 2024.

Goodenough, K., Millar, I., Strachan, R., Krabbendam, M., and Evans, J.: Timing of regional deformation and development of the Moine Thrust Zone in the Scottish Caledonides: constraints from the U–Pb geochronology of alkaline intrusions, J. Geol. Soc. London, 168, 99–114, 2011.

Guo, M., Zhang, J., Qian, J., Yin, C., Gao, P., Hsia, J., Zhang, S., and Yu, C.: Ultrahigh-temperature metamorphism of the felsic granulites in the eastern North China Craton and their implications on the Neoarchean tectonic regime, Lithos, 468, 107516, https://doi.org/10.1016/j.lithos.2024.107516, 2024.

Hanson, G. and Gast, P.: Kinetic studies in contact metamorphic zones, Geochim. Cosmochim. Ac., 31, 1119–1153, 1967.

Harrison, T. M. and Clarke, G. K.: A model of the thermal effects of igneous intrusion and uplift as applied to Quottoon pluton, British Columbia, Can. J. Earth Sci., 16, 411–420, 1979.

Hogmalm, K. J., Zack, T., Karlsson, A. K.-O., Sjöqvist, A. S., and Garbe-Schönberg, D.: In situ Rb–Sr and K–Ca dating by LA-ICP-MS/MS: an evaluation of N_2O and SF_6 as reaction gases, J. Anal. Atom. Spectrom., 32, 305–313, 2017.

Holness, M. B. and Clemens, J. D.: Partial melting of the Appin Quartzite driven by fracture-controlled H2O infiltration in the aureole of the Ballachulish Igneous Complex, Scottish Highlands, Contrib. Mineral. Petr., 136, 154–168, 1999.

Jenkin, G. R., Ellam, R. M., Rogers, G., and Stuart, F. M.: An investigation of closure temperature of the biotite Rb–Sr system: The importance of cation exchange, Geochim. Cosmochim. Ac., 65, 1141–1160, 2001.

Jenkin, G. R. T., Rogers, G., Fallick, A. E., and Farrow, C. M.: Rb–Sr closure temperatures in bi-mineralic rocks: a mode effect and test for different diffusion models, Chem. Geol., 122, 227–240, https://doi.org/10.1016/0009-2541(95)00013-C, 1995.

Kelly, E., Carlson, W., and Connelly, J.: Implications of garnet resorption for the Lu–Hf garnet geochronometer: an example from the contact aureole of the Makhavinekh Lake Pluton, Labrador, J. Metamorph. Geol., 29, 901–916, 2011.

Kutzschbach, M. and Glodny, J.: LA-ICP-MS/MS-based Rb–Sr isotope mapping for geochronology, J. Anal. Atom. Spectrom., 39, 455–477, 2024.

Larson, K. P., Shrestha, S., Button, M., Cottle, J. M., and Barnes, C. J.: The Effect of Crystal Orientation on In situ Rb–Sr Mica Geochronology, Geostand. Geoanal. Res., 49, 705–713, 2025.

Lightfoot, P. C., Keays, R. R., Evans-Lamswood, D., and Wheeler, R.: S saturation history of Nain Plutonic Suite mafic intrusions: origin of the Voisey's Bay Ni–Cu–Co sulfide deposit, Labrador, Canada, Miner. Deposita, 47, 23–50, 2012.

Ludwig, K. R.: User's manual for Isoplot 3.75: A geochronological toolkit for Microsoft Excel, Berkeley Geochronology Center Special Publication, 5, 75, 2012.

Mariga, J., Ripley, E., and Li, C.: Petrologic evolution of gneissic xenoliths in the Voisey's Bay Intrusion, Labrador, Canada: Mineralogy, reactions, partial melting, and mechanisms of mass transfer, Geochem. Geophy. Geosy., 7, https://doi.org/10.1029/2005GC001184, 2006.

McFarlane, C., Carlson, W., and Connelly, J.: Prograde, peak, and retrograde P–T paths from aluminium in orthopyroxene: High-temperature contact metamorphism in the aureole of the Makhavinekh Lake Pluton, Nain Plutonic Suite, Labrador, J. Metamorph. Geol., 21, 405–423, 2003.

McFarlane, C. R. and Harrison, T. M.: Pb-diffusion in monazite: constraints from a high-T contact aureole setting, Earth Planet. Sc. Lett., 250, 376–384, 2006.

McFarlane, C. R., Connelly, J. N., and Carlson, W. D.: Monazite and xenotime petrogenesis in the contact aureole of the Makhavinekh Lake Pluton, northern Labrador, Contrib. Mineral. Petr., 148, 524–541, 2005a.

McFarlane, C. R., Connelly, J. N., and Carlson, W. D.: Intracrystalline redistribution of Pb in zircon during high-temperature contact metamorphism, Chem. Geol., 217, 1–28, 2005b.

Meija, J., Coplen, T. B., Berglund, M., Brand, W. A., Bièvre, P. D., Gröning, M., Holden, N. E., Irrgeher, J., Loss, R. D., Walczyk, T., and Prohaska, T.: Isotopic compositions of the elements 2013 (IUPAC Technical Report), Pure Appl. Chem., 88, 293–306, https://doi.org/10.1515/pac-2015-0503, 2016.

Mengel, F. and Rivers, T.: Metamorphism in the Paleoproterozoic Torngat Orogen, Labrador: Petrology and P-T-t paths of amphibolite- and granulite-facies rocks across the Komaktorvik shear zone, Can. Mineral., 35, 1137–1160, 1997.

Mengel, F., Rivers, T., and Reynolds, P.: Lithotectonic elements and tectonic evolution of Torngat Orogen, Saglek Fiord, northern Labrador, Can. J. Earth Sci., 28, 1407–1423, 1991.

Müller, W., Mancktelow, N. S., and Meier, M.: Rb–Sr microchrons of synkinematic mica in mylonites: an example from the DAV fault of the Eastern Alps, Earth Planet. Sc. Lett., 180, 385–397, 2000.

Muñoz-Montecinos, J., Giuliani, A., Oesch, S., Volante, S., Peters, B., and Behr, W.: In situ rubidium–strontium geochronology of white mica in young metamafic and metasomatic rocks from Syros: testing the limits of laser-ablation triple-quadrupole inductively coupled plasma mass spectrometer mica dating using different anchoring approaches, Geochronology, 6, 585–605, https://doi.org/10.5194/gchron-6-585-2024, 2024.

Nebel, O.: Rb–Sr dating, in: Encyclopedia of scientific dating methods, Springer, 686–698, https://doi.org/10.1016/j.jsg.2023.104947, 2015.

Olierook, H. K. H., Rankenburg, K., Ulrich, S., Kirkland, C. L., Evans, N. J., Brown, S., McInnes, B. I. A., Prent, A., Gillespie, J., McDonald, B., and Darragh, M.: Resolving multiple geological events using in situ Rb–Sr geochronology: implications for metallogenesis at Tropicana, Western Australia, Geochronology, 2, 283–303, https://doi.org/10.5194/gchron-2-283-2020, 2020.

Paton, C., Hellstrom, J. C., Paul, B., Woodhead, J. D., and Hergt, J. M.: Iolite: Freeware for the visualisation and processing of mass spectrometric data, J. Anal. Atom. Spectrom., 26, 2508–2518, 2011.

Percival, J. and Peterman, Z.: Rb–Sr biotite and whole-rock data from the Kapuskasing uplift and their bearing on the cooling and exhumation history, Can. J. Earth Sci., 31, 1172–1181, 1994.

Ribeiro, B. V., Kirkland, C. L., Finch, M. A., Faleiros, F. M., Reddy, S. M., Rickard, W. D., and Hartnady, M. I.: Microstructures, geochemistry, and geochronology of mica fish: Review and advances, J. Struct. Geol., 175, 104947, https://doi.org/10.1007/978-94-007-6304-3_116, 2023.

Rivers, T., Mengel, F., Scott, D. J., Campbell, L. M., and Goulet, N.: Torngat Orogen – a Palaeoproterozoic example of a narrow doubly vergent collisional orogen, Geological Society, London, Special Publications, 112, 117–136, 1996.

Ryan, B.: Makhavinekh lake pluton, Labrador, Canada: geological setting, subdivisions, mode of emplacement, and a comparison with Finnish rapakivi granites, Precambrian Res., 51, 193–225, 1991.

Scott, D. J.: An overview of the U–Pb geochronology of the Paleoproterozoic Torngat Orogen, Northeastern Canada, Precambrian Res., 91, 91–107, 1998.

Scott, D. J. and Machado, N.: UPb geochronology of the northern Torngat Orogen, Labrador, Canada: a record of Palaeoproterozoic magmatism and deformation, Precambrian Res., 70, 169–190, 1995.

Sneeringer, M., Hart, S. R., and Shimizu, N.: Strontium and samarium diffusion in diopside, Geochim. Cosmochim. Ac., 48, 1589–1608, 1984.

Sousa, J., Kohn, M. J., Schmitz, M. D., Northrup, C. J., and Spear, F.: Strontium isotope zoning in garnet: implications for metamorphic matrix equilibration, geochronology and phase equilibrium modelling, J. Metamorph. Geol., 31, 437–452, 2013.

Tajčmanová, L., Connolly, J., and Cesare, B.: A thermodynamic model for titanium and ferric iron solution in biotite, J. Metamorph. Geol., 27, 153–165, 2009.

Tan, H. M. R., Huang, X.-W., Meng, Y.-M., Xie, H., and Qi, L.: Multivariate statistical analysis of trace elements in apatite: Discrimination of apatite with different origins, Ore Geol. Rev., 153, 105269, https://doi.org/10.1016/j.oregeorev.2022.105269, 2023.

Tettelaar, T. and Indares, A.: Granulite-facies regional and contact metamorphism of the Tasiuyak paragneiss, northern Labrador: textural evolution and interpretation, Can. J. Earth Sci., 44, 1413–1437, 2007.

Thirlwall, M. and Burnard, P.: Pb–Sr–Nd isotope and chemical study of the origin of undersaturated and oversaturated shoshonitic magmas from the Borralan pluton, Assynt, NW Scotland, J. Geol. Soc. London, 147, 259–269, 1990.

Van Breemen, O., Aftalion, M., and Johnson, M.: Age of the Loch Borrolan complex, Assynt, and late movements along the Moine Thrust Zone, J. Geol. Soc. London, 136, 489–495, 1979.

Van Kranendonk, M. J.: Tectonic evolution of the Paleoproterozoic Torngat Orogen: Evidence from pressure-temperature-time-deformation paths in the North River map area, Labrador, Tectonics, 15, 843–869, 1996.

Vermeesch, P.: IsoplotR: A free and open toolbox for geochronology, Geosci. Front., 9, 1479–1493, 2018.

von Blanckenburg, F., Villa, I., Baur, H., Morteani, G., and Steiger, R.: Time calibration of a PT-path from the Western Tauern Window, Eastern Alps: the problem of closure temperatures, Contrib. Mineral. Petr., 101, 1–11, 1989.

Walawender, M., Gastil, R., Clinkenbeard, J., McCormick, W., Eastman, B., Wernicke, R., Wardlaw, M., Gunn, S., and Smith, B.: Origin and evolution of the zoned La Posta-type plutons, eastern Peninsular Ranges batholith, southern and Baja California, Geological Society of America Memoir, Boulder, Colorado, https://doi.org/10.1130/MEM174-p1, 1990.

Whitney, D. L. and Evans, B. W.: Abbreviations for names of rock-forming minerals, Am. Mineral., 95, 185–187, 2010.

Willigers, B., Mezger, K., and Baker, J.: Development of high precision Rb–Sr phlogopite and biotite geochronology; an alternative to $^{40}Ar/^{39}Ar$ tri-octahedral mica dating, Chem. Geol., 213, 339–358, 2004.

Wohletz, K., Civetta, L., and Orsi, G.: Thermal evolution of the Phlegraean magmatic system, J. Volcanol. Geoth. Res., 91, 381–414, 1999.

Yang, L., Wang, J.-M., Liu, X.-C., Khanal, G. P., and Wu, F.-Y.: Sr–Nd–Hf Isotopic Disequilibrium during the partial melting of metasediments: insight from Himalayan leucosome, Front. Earth Sci., 10, 891960, https://doi.org/10.3389/feart.2022.891960, 2022.

Zack, T. and Hogmalm, K. J.: Laser ablation Rb/Sr dating by online chemical separation of Rb and Sr in an oxygen-filled reaction cell, Chem. Geol., 437, 120–133, 2016.